Cell Imaging

Tunable Imaging of Cells Labeled with MRI-PARACEST Agents**

Silvio Aime, Carla Carrera, Daniela Delli Castelli, Simonetta Geninatti Crich, and Enzo Terreno*

Magnetic resonance imaging (MRI) modality is ideally suited to monitor cell tracking in vivo, as it exhibits superb spatial resolution.[1] Two classes of MRI probes are currently used in cell-labeling procedures: iron oxide nanoparticles and Gd^{III} chelates, both of which act as relaxation enhancers of water protons. The use of the former class in cell-tracking studies is well established.[2–5] Until now, the latter class has enjoyed only limited use in cell labeling, although it has been shown that incubation of stem cells in the presence of stable Gd^{III} chelates can give good internalization results.[6–8] The metal chelate units are usually confined inside endosomes in the perinuclear region; in this form, they do not affect cell viability. Moreover, it has been found recently that stem cells labeled with [Gd(hpdo3A)] (a clinically approved agent) are MRI-detectable up to two weeks after implantation.[8] The main drawback of both classes of agents is that visualization of more than one ensemble of labeled cells in each cell-tracking experiment is not possible.

Recently, a new class of MRI contrast agents has been proposed: the so-called CEST (chemical exchange saturation transfer) agents.[9] These systems contain at least one pool of exchangeable protons, which upon irradiation at their absorption frequency, transfer saturated magnetization to the bulk water signal (Figure 1). Thus, members of this class of agent act as negative agents (analogous to iron oxide particles) by decreasing the intensity of the water signal through the transfer of saturated magnetization. Interestingly, these agents display their effect in MRI only when the irradiation frequency is set at the value that corresponds to the absorption frequency of their mobile protons. The use of lanthanide(III) paramagnetic chelates (PARACEST agents) has been shown to be particularly beneficial, as the paramagnetic ion induces a large shift in the resonance of nuclei surrounding it.[10] In fact, a large chemical-shift difference between the exchangeable protons and bulk water resonances allows the exploitation of larger values of exchange rates (k_{ex}) which, in turn, results in a more efficient transfer of saturated magnetization. Moreover, the use of PARACEST agents endowed with markedly different chemical-shift values of the

[*] Prof. S. Aime, Dr. C. Carrera, Dr. D. Delli Castelli, Dr. S. Geninatti Crich, Dr. E. Terreno
Dipartimento di Chimica I.F.M.
Via P. Giuria 7, 10125 Torino (Italy)
Fax: (+39) 011-670-7855
E-mail: silvio.aime@unito.it

[**] Financial support from Bracco Imaging S.p.A., and MIUR (FIRB) are gratefully acknowledged. This work has been carried out under the framework of the EU-COST D 18 Action and EMIL-NoE.

 DOI: 10.1002/ange.200462566

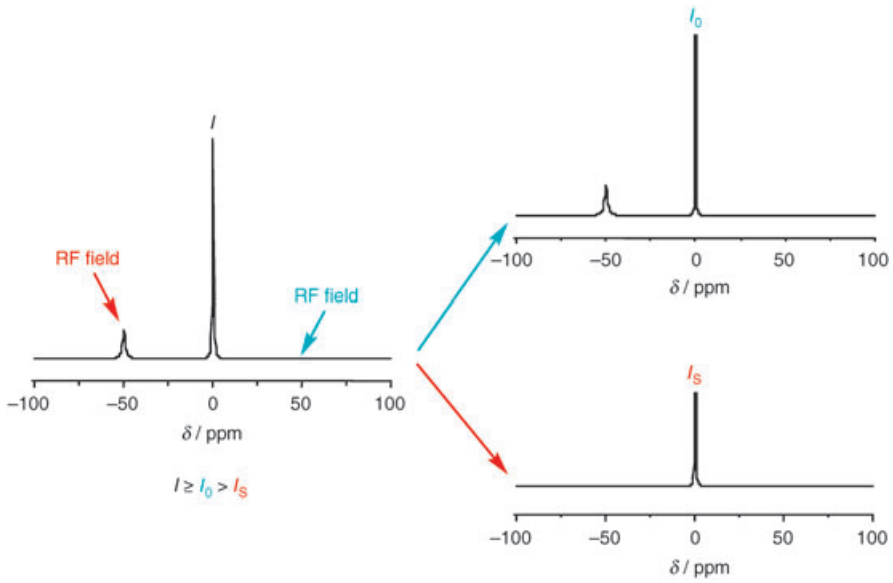

Figure 1. A given RF field is applied at the resonance frequency of the exchangeable protons of the CEST agent (red). The saturation of this resonance is transferred to the resonance of the bulk water protons ($I_S < I$). As the RF field may perturb the intensity of the signal of water protons, the same RF field is applied at a frequency symmetrically opposite to that of the CEST agent (blue). Therefore, the net saturation transfer is calculated as $ST = 1-(I_S/I_0)$.

exchangeable protons allows them to be visualized at will by a selection of the proper irradiation frequency.

The PARACEST agents used in the study reported herein are shown below. The two metal complexes share the same

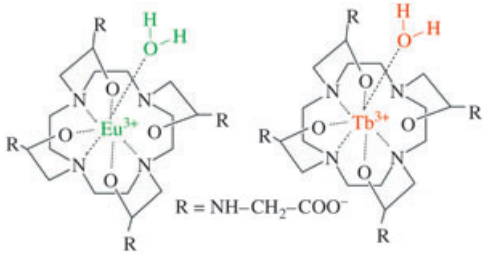

ligand (dotamGly) and therefore have the same chemical and biological behavior, whereas their ^{1}H NMR spectra are markedly different, as expected from the different magnetic characteristics of the two lanthanide(III) ions.[11] Both complexes contain two pools of exchangeable protons: the metal-coordinated water protons and the amide protons.[12] Herein, the presence of both PARACEST agents was visualized by using the water resonances that were the most dramatically shifted. Thus, by irradiation 50 ppm downfield from the resonance of bulk water protons, it is possible to detect the response from the Eu^{III} complex, whereas a switch to an irradiation frequency of −600 ppm from bulk water permits detection of the Tb^{III} complex instead.

Figure 2 shows the results obtained from a phantom that comprises four capillaries: A) phosphate buffer, B) [Tb(dotamGly)] (2 mM) C) [Eu(dotamGly)] (2 mM), and D) a mixture of the two complexes at a concentration of 1 mM. The CEST-MR images represent the subtraction of two images that differ only in the frequency of irradiation. In one experiment (on-image) the irradiation was performed at the appropriate resonance for the exchangeable protons of interest: 50 ppm for the Eu^{III}-containing complex and −600 ppm for the Tb^{III} analogue. In the other experiment (off-image) the irradiation was carried out for the Eu^{III}- and Tb^{III}-containing complexes at −50 ppm and 600 ppm, respectively. The latter experiment was necessary, as the irradiation pulse itself can decrease the intensity of the water signal through direct saturation effects. As this phenomenon strictly depends on the absolute value of the irradiation frequency, the real saturation transfer of the PARACEST system is determined by a comparison of the on- and off-images.[10–12] The CEST-MR images shown in Figure 2 strongly confirm that upon irradiation at 600 ppm (absolute value), only the solution that contains [Tb(dotamGly)] is visualized through the appearance of dark spots (colored in red in the figure), whereas solutions containing [Eu(dotamGly)] remain unaffected and indistinguishable from the control

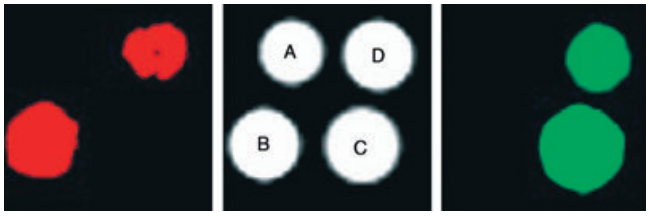

Figure 2. Middle image: MRI (7 T) of a phantom made of four capillaries that contain: A) PBS buffer, B) [Tb(dotamGly)] (2 mM), C) [Eu(dotamGly)] (2 mM), D) [Tb(dotamGly)] and [Eu(dotamGly)] (1 mM each). Right and left: CEST-MR difference images obtained by irradiation of the metal-bound water protons of [Tb(dotamGly)] (left) and [Eu(dotamGly)] (right); the contrast has been arbitrarily colored in red and green, respectively; dotamGly = the tetraglycineamide derivative of dota: 1,4,7,10-tetraazacyclododecane-1,4,7,10-tetraacetic acid.

(spot A)). The reverse result occurs upon irradiation at 50 ppm (absolute value), in which case only the presence of the Eu^{III} complex is detected (green spots). The extent of the saturation transfer is proportional to the concentration of the PARACEST agent. Consequently, tubes containing solution concentrations of 2 mM are more intense. Quantitatively, the decrease in the intensity of the water signal upon irradiation of the water bound to the Eu^{III} complex was 4% (1 mM) and 12% (2 mM), whereas the corresponding values for Tb^{III} analogue were 8% (1 mM) and 12% (2 mM).

Cell labeling with the two PARACEST probes was carried out by incubation of $\approx 10^6$ HTC (rat hepatoma) tumor cells in the presence of each complex (40 mM) in the incubation medium for 6 h. A rough estimate of the amount of internalized complex was determined by performing the same incubation procedure with the [Gd(dotamGly)] com-

plex. After incubation, the cells were washed three times and the amount of internalized Gd^{III} was determined by relaxometric measurement of the cell lysates obtained after mineralization with HCl (3 M) in a sealed vial at 120 °C overnight.[8] The amount of Gd^{III} complex internalized upon incubation at 40 mM, $\approx 8 \times 10^9$ molecules/cell, is a good parallel to the results reported for the internalization of [Gd(hpdo3A)] into endothelial progenitor cells.[8]

Cells incubated in the presence of [Eu(dotamGly)] and [Tb(dotamGly)] were collected as pellets after three wash steps with DMEM (DMEM = Dulbecco modified Eagle medium). Next, a phantom similar to that shown in Figure 2 was prepared, in which spot A) contained a pellet of unlabeled HTC cells, B) a pellet of Tb^{III}-labeled cells, C) pelleted cells labeled with the Eu^{III} complex, and D) a pellet obtained from a mixture of cells of spots B) and C). As described above for the aqueous solutions, the irradiation frequency was initially set at 600 ppm and then at 50 ppm (absolute values). Again, by irradiation at 600 ppm, cells that contained Tb^{III} complex were detected exclusively, whereas a switch of the irradiation frequency to 50 ppm showed a response only from Eu^{III}-complex-containing cells (Figure 3). The decrease in the intensity of the water signal was 4% (pellet D)) and 12% (pellet C)) upon irradiation at ± 50 ppm, and 3.5% (pellet D)) and 11.2% (pellet B)) upon irradiation at ± 600 ppm.

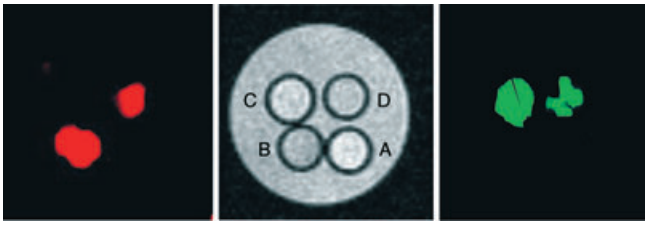

Figure 3. Middle image: MRI (7 T) of a phantom made of four capillaries that contain: A) unlabeled HTC cells, B) HTC cells labeled with [Tb(dotamGly)], C) HTC cells labeled with [Eu(dotamGly)], D) cellular pellet obtained from a mixture of pellets of spots B) and C). Right and Left: CEST-MR difference images obtained by irradiation of the metal-bound water protons of [Tb(dotamGly)] (left) and [Eu(dotamGly)] (right); the contrast has been arbitrarily colored in red and green, respectively.

In summary, these studies establish and validate a novel and powerful tool for the detection of different ensembles of labeled cells, and provide a rationale for the development of analogous procedures for detection in vivo. Internalization of the PARACEST agents by pinocytosis appears to be a safe and efficient route for cellular labeling, as it allows entrapment of high quantities of the agent, sufficient for CEST-MRI detection. Furthermore, as it has been shown that PARACEST agents can be designed to respond to a specific parameter of the microenvironment in which they are distributed,[13–15] a number of applications can be envisaged that expand the potential of MRI techniques in the field of cell tracking. Finally, this approach may provide useful insight for the evaluation of novel cell-based therapies in vivo, as the fates of differently labeled cells that are administered serially can be followed.

Experimental Section

Chemicals: [Eu(dotamGly)] and [Tb(dotamGly)] were synthesized according to literature protocol.[11]

Cells: HTC cells (rat tumor hepatoma cells) were provided by the ICLC (National Institute for Cancer Research, Genova, Italy) and were labeled with [Eu(dotamGly)] or [Tb(dotamGly)] probes according to methods previously described.[8] Briefly, $\approx 5–6 \times 10^6$ cells were incubated at 37 °C for 6 h in a culture medium containing the labeling probe (40 mM). The cells were then washed three times with ice-cold PBS (phosphate-buffered saline) (10 mL) and detached by the addition of trypsin and EDTA (ethylenediaminetetraacetic acid).

MRI: All CEST-MR images were acquired on a Bruker Avance 300 spectrometer equipped with a MICRO 2.5 microimaging probe (resonator ID: 10 mm). Each CEST-MR image is the difference of two spin echo images (TR/TE/NE = 6 s/3.5 ms/1) that differ in the offset of the irradiation pulse ($I_S - I_0$, Figure 1). The total irradiation time was 2 s. The irradiation pulse consisted of a train of sinc 3 pulses (irradiation power ≈ 250 μT) with a duration of 1 ms for the Eu^{III} complex and 250 μs for the Tb^{III} complex. The interpulse delay was 10 μs. Other parameters: 64×64 isotropic matrix; FOV 6×6 mm; slice thickness = 2 mm.

Received: November 10, 2004
Published online: February 21, 2005

Keywords: imaging agents · lanthanides · magnetic properties · proton exchange · saturation transfer

[1] P. A. Rinck, *Magnetic Resonance in Medicine*, ABW Wissenschaftsverlag GmbH, Berlin, **2003**.
[2] P. Jendelova, V. Herynek, L. Urdzikova, K. Glogarova, J. Kroupova, B. Andersson, V. Bryja, M. Burian, M. Hajek, E. Sykova, *J. Neurosci. Res.* **2004**, 76, 232–243.
[3] J. A. Frank, B. R. Miller, A. S. Arbab, H. A. Zywicke, E. K. Jordan, B. K. Lewis, L. H. Bryant, J. W. M. Bulte, *Radiology* **2003**, *228*, 480–487.
[4] K. A. Hinds, J. M. Hill, E. M. Shapiro, M. O. Laukkanen, A. C. Silva, C. A. Combs, T. R. Varney, R. S. Balaban, A. P. Koretsky, C. E. Dunbar, *Blood* **2003**, *102*, 867–872.
[5] M. Hoehn, E. Kustermann, J. Blunk, D. Wiedermann, T. Trapp, S. Wecker, M. Focking, H. Arnold, J. Hescheler, B. K. Fleischmann, W. Schwindt, C. Buhrle, *Proc. Natl. Acad. Sci. USA* **2002**, *99*, 16267–16272.
[6] M. Rudelius, H. E. Daldrup-Link, U. Heinzmann, G. Piontek, M. Settles, T. M. Link, J. Schlegel, *Eur. J. Nucl. Med. Mol. Imaging* **2003**, *30*, 1038–1044.
[7] M. Modo, K. Mellodew, D. Cash, S. E. Fraser, T. J. Meade, J. Price, S. C. R. Williams, *Neuroimage* **2004**, *21*, 311–317.
[8] S. Geninatti Crich, L. Biancone, V. Cantaluppi, G. Esposito, S. Russo, G. Camussi, S. Aime, *Magn. Reson. Med.* **2004**, *51*, 938–944.
[9] K. M. Ward, A. H. Aletras, R. S. Balaban, *J. Magn. Reson.* **2000**, *143*, 79–87.
[10] S. Zhang, M. Merritt, D. E. Woessner, R. E. Lenkinski, A. D. Sherry, *Acc. Chem. Res.* **2003**, *36*, 783–790.
[11] S. Aime, A. Barge, D. Delli Castelli, F. Fedeli, A. Mortillaro, F. U. Nielsen, E. Terreno, *Magn. Reson. Med.* **2002**, *47*, 639–648.
[12] E. Terreno, D. Delli Castelli, G. Cravotto, L. Milone, S. Aime, *Invest. Radiol.* **2004**, *39*, 235–243.
[13] S. Aime, D. Delli Castelli, E. Terreno, *Angew. Chem.* **2002**, *114*, 4510–4512; *Angew. Chem. Int. Ed.* **2002**, *41*, 4334–4336.
[14] S. Aime, D. Delli Castelli, F. Fedeli, E. Terreno, *J. Am. Chem. Soc.* **2002**, *124*, 9364–9365.
[15] S. Zhang, R. Trokowski, A. D. Sherry, *J. Am. Chem. Soc.* **2003**, *125*, 15288–15289.

